SB

PSI-PR-94-38
December 1994

PAUL SCHERRER INSTITUT

Muonic Atom Emission into Vacuum from Inhomogeneous Mixtures of Hydrogen Isotopes and Kinetics of Muon Catalyzed Fusion in Multilayered Target Systems

sw 9502

V.E. Markushin

Paul Scherrer Institut
CH-5232 Villigen PSI, Switzerland

Paul Scherrer Institut
Würenlingen and Villigen
CH-5232 Villigen / PSI

Telephone 056 99 21 11
Telefax 056 98 23 27
Telex 82 74 14 psi ch

Muonic Atom Emission into Vacuum from Inhomogeneous Mixtures of Hydrogen Isotopes and Kinetics of Muon Catalyzed Fusion in Multilayered Target Systems

V.E. Markushin[1]

Paul Scherrer Institute, Villigen PSI, CH-5232, Switzerland

Abstract

The emission of μt atoms from a solid hydrogen-tritium target covered with a deuterium layer and the formation of $dt\mu$ molecules in deuterium layers separated by a vacuum gap have been investigated with a kinetics model. It is shown that with a proper choice of the setup parameters the dt fusion time spectra can be used to obtain information on muon transfer from a proton to a triton, the Ramsauer-Townsend effect in $\mu t + p$ scattering, $\mu t + d$ scattering, resonant $dt\mu$ molecule formation, and nonresonant $pp\mu$ formation.

[1]On leave from Russian Research Center, Kurchatov Institute, Moscow 123182, Russia.

1 Introduction

Current interest in muon catalyzed fusion (μCF) spreads from fundamental problems focused on the interplay of strong, electromagnetic, and weak interactions to possible applications for neutron and energy production (see [1, 2, 3, 4] and references therein). The key process in μCF is the formation of muonic molecules, in which the nuclear fusion occurs with high probability due to muon screening of the Coulomb repulsion between nuclei. While a high efficiency of the $dt\mu$ fusion cycle has been predicted theoretically and proven by experiment (more than 100 dt fusions per muon can be achieved in a dense DT mixture, see [5, 6] and references therein), the kinetics of the μCF cycle is not yet completely investigated. Of particular interest is the resonant formation of muonic molecules [7, 8, 9, 10, 11], however, the energy dependence of the formation rates has been studied until now only indirectly [12, 13, 14, 15] because of the lack of muonic atom beams.

This obstacle is overcome in a TRIUMF experiment [16, 17] in which a new target system is used to produce muonic atoms emitted in vacuum as an atomic beam. The negative muons are stopped in a solid layer composed of protium with a small admixture of deuterium or tritium and captured mainly by protons, thus forming neutral μp atoms, while μd and μt atoms are produced in the reactions of the muon transfer to the heavier hydrogen isotopes. The high efficiency of muonic atom emission occurs due to the Ramsauer-Townsend effect in $\mu d + p$ and $\mu t + p$ collisions, which makes the mean free path of the muonic atoms abnormally large in the energy range of a few electron volts. Known since the first experimental observation of μCF [18] and studied theoretically [19, 20, 21], this effect, however, has never been measured in detail.

The energy of emitted atoms can be measured by time of flight (ToF) for each muonic atom travelling through a vacuum gap to the reaction target where muonic molecule formation and nuclear fusion take place. With a proper setup one can isolate muon molecular formation from the other parts of the μCF cycle [17]. In order to determine the optimum experimental conditions and develop the method of data analysis, a detailed theoretical framework is required. In particular, the following problems must be investigated:

1. The dependence of the muonic atoms yield on the thickness and composition of the production target.

2. The energy distribution of the emitted muonic atoms and its dependence on the setup parameters.

3. The feasibility of measurements of the rates of selected processes, such as muon transfer, elastic collisions, and resonant and nonresonant formation of muonic molecules.

Most of these problems are connected with the kinetics of 'hot', *i.e.* nonthermalized, muonic atoms. While the kinetics of 'hot' atoms in homogeneous mixtures of hydrogen isotopes were studied recently for various experimental conditions [22, 23, 24, 25, 26, 27, 28], very few results are available for nonhomogeneous systems [17]. The goal of this paper is to provide a detailed theoretical study of muonic atom emission from inhomogeneous

mixtures of hydrogen isotopes and muon catalyzed fusion in multilayered systems. The paper is arranged as follows: the kinetics problem is described in Sec. 2, the solutions to the kinetics problem are discussed in Sec. 3, and Section 4 contains the summary of the results. The present work is focused on the μt atoms, as they are of primary importance for the $dt\mu$ branch of muon catalyzed fusion. The results for μd atoms will be published elsewhere.

Unless otherwise stated, all collisional rates and ranges are normalized to the liquid hydrogen density (LHD) $N_0 = 4.25 \cdot 10^{22}\,\mathrm{cm}^{-3}$. Material thicknesses are measured in the units of mass per area, which are connected with the units of length as follows: 1 mm of solid hydrogen (protium) (1.2 LHD) corresponds to 8.5 mg/cm^2 and 1 mm of solid deuterium corresponds to 19.4 mg/cm^2.

2 Kinetics

2.1 Kinetics Scheme

In the present study we take the TRIUMF setup [16, 17] as a reference system; however, our analysis is not restricted by this case, and the problem involved is treated in a wider context. The multilayered target system used in the TRIUMF experiment consists of a μt production target and a main fusion target separated by a vacuum gap, as is shown schematically in Fig. 1(a).

The production target is a layer of solid protium with a small admixture of tritium, placed on a gold foil. The muons are stopped in the production target, forming mainly μp atoms which produce μt atoms in the muon transfer reaction

$$\mu p + t \rightarrow \mu t + p \tag{1}$$

The kinetic energy of the μt atom is about 45 eV, which is mainly determined by the recoil due to the difference of the binding energies of $(\mu t)_{1S}$ and $(\mu p)_{1S}$. Slowing down in elastic collisions, the μt can reach the energy region (5 – 15) eV where the cross section of elastic $\mu t + p$ scattering is abnormally small due to the Ramsauer-Townsend effect. According to the theoretical calculations [19, 20], the S-wave scattering amplitude has a zero at $E_{CMS} = 3\,\mathrm{eV}$ and the elastic cross section is $\sigma^{t}_{\mu t+p}(E_{CMS} = 3\,\mathrm{eV}) = 1.7 \cdot 10^{-21}$ cm^2, the corresponding range in hydrogen being 0.14 mm (1.2 mg/cm^2). Thus a significant fraction of μt can leave the H-T layer before the muon decays or the $pt\mu$ molecule formation occurs. For an H-T layer of up to about 3 mg/cm^2 (0.4 mm) one can also get a uniform muon stopping distribution along the Z-axis, making the initial conditions of the kinetics problem well defined.

The production target can be covered with an overlayer of deuterium ("upstream" or US) , which is much thinner than the protium layer but sufficient for degrading the μt atoms before they escape into the vacuum. By varying the thickness of the US overlayer one can change the kinetic energy distribution of the emitted muonic tritium.

The secondary target is a solid deuterium layer ("downstream" or DS) placed on a gold foil at a distance l from the μt production target. With a proper choice of the setup

parameters the measured time distribution of the fusion events in the DS target is mainly determined by the time of flight of the projectiles.

In Monte Carlo calculations, for the sake of saving CPU time, we assumed the configuration of the setup to be symmetric with respect to the central plane of the H-T layer (Fig. 1), so that all theoretical yields must be reduced by a factor of 2 when compared with the TRIUMF experiment.

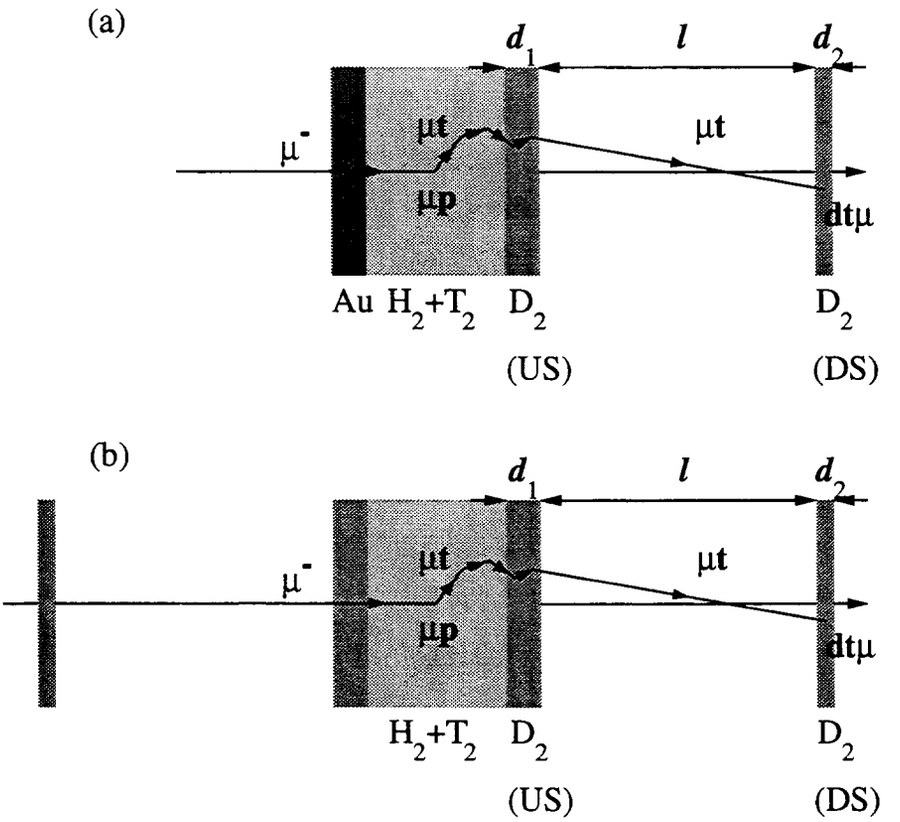

Figure 1: The scheme of the setup: (a) TRIUMF experiment; (b) Monte Carlo simulation.

The scheme of kinetics is shown in Fig. 2. Density ϕ, isotope fractions C_a $(a = p, d, t)$, and molecular concentration C_{D_2} are functions of space position according to Fig. 1(b)[2]. At low tritium fractions the μt atoms are mainly formed by transfer from hydrogen, which competes with $pp\mu$ molecule formation. The μt atoms are formed in the hyperfine structure states $F = 0, 1$ according to their statistical weights. The muonic tritium slows down in collisions with hydrogen, deuterium, and tritium. The $dt\mu$ molecule formation is strongly dependent on the energy and spin of μt and the target temperature. The $pt\mu$ formation is weakly energy dependent.

[2] $\phi = 1$ corresponds to LHD, $C_p + C_d + C_t = 1$, $C_{D_2} = 1$ for pure deuterium.

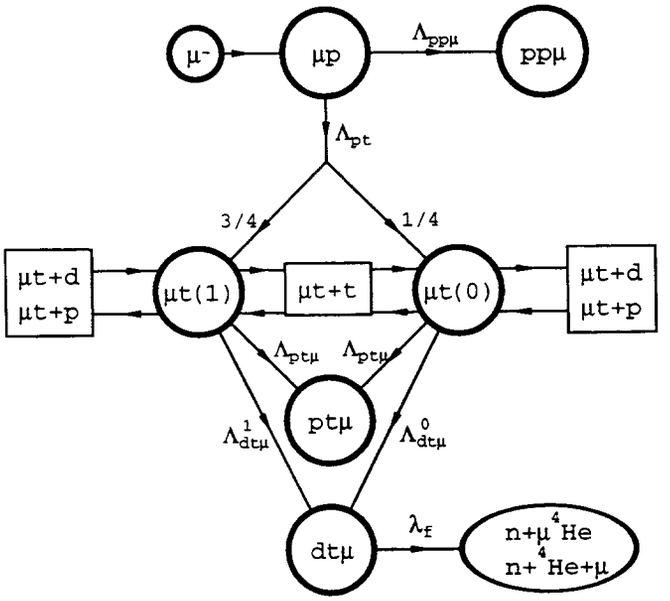

Figure 2: The scheme of the kinetics used in Monte Carlo simulations. The transition rates are defined as follows: the $\mu p \rightarrow \mu t$ transfer rate $\Lambda_{pt} = \lambda_{pt}\phi C_t$, the $pp\mu$ formation rate $\Lambda_{pp\mu} = \lambda_{pp\mu}\phi C_p$, the $pt\mu$ formation rate $\Lambda_{pt\mu} = \lambda_{pt\mu}\phi C_p$, the $dt\mu$ formation rates $\Lambda^F_{dt\mu} = \lambda^F_{dt\mu}\phi C_{D_2}$, the $dt\mu$ fusion rate λ_f, and the other rates are explained in the text.

The following approximations have been used in the calculations.

1. Only muon stops in H-T mixture are considered, and μd formation in the deuterium layers is neglected. Direct capture by tritium is also neglected.

2. Diffusion of μp atoms is neglected, so that μt formation is uniformly distributed in the H-T layer, and the initial μt energy is assumed to be $E_i = 44.5\,\mathrm{eV}$, corresponding to the transfer at rest.

3. Molecule and temperature effects in μt scattering from hydrogen isotopes were neglected.

2.2 Kinetics Rates

The total and differential cross sections for μt+p, μt+d, and μt+t collisions were calculated using T-matrixes from [19] for the partial waves $L = 0, 1, 2$. The total collisional rates for $\mu t + p$ and $\mu t + t$ calculated with elastic cross sections at liquid hydrogen density are shown in Fig. 3.

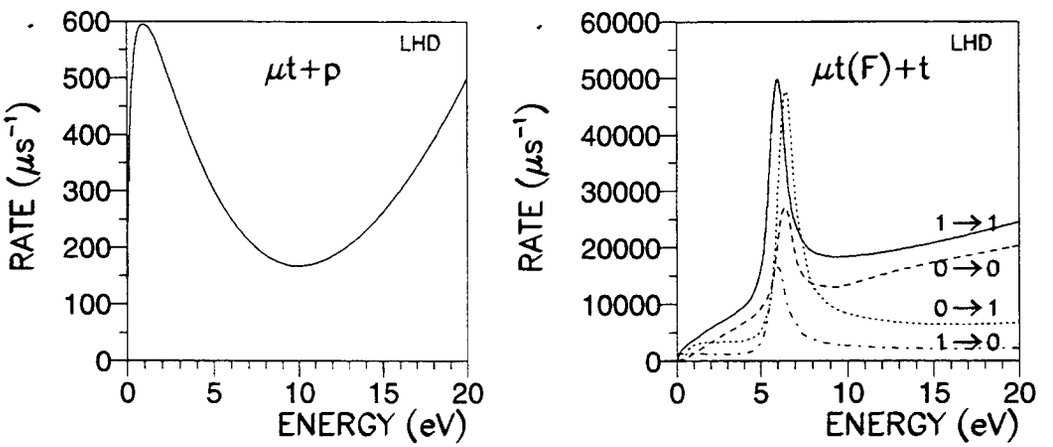

Figure 3: The rates of the $\mu t + p$ and $\mu t(F) + t \to \mu t(F') + t$ collisions *vs.* laboratory energy of the μt atom (LHD).

The effective $dt\mu$ formation rates in the reaction

$$\mu t(F) + D_2 \to [(dt\mu)_{(Jv)=(11)} d2e] \tag{2}$$

at $T = 3\,\mathrm{K}$, with the back decay corrections included, were taken from [10]. The $dt\mu$ resonant formation rates are compared with the rates of $\mu t + d$ collisions in Fig. 4.

The following rates were considered energy independent in the present calculations: the $pp\mu$ formation rate $\lambda_{pp\mu} = 1.9\,\mu\mathrm{s}^{-1}$ [29, 31], the $pt\mu$ formation rate $\lambda_{pt\mu} = 6.5\,\mu\mathrm{s}^{-1}$

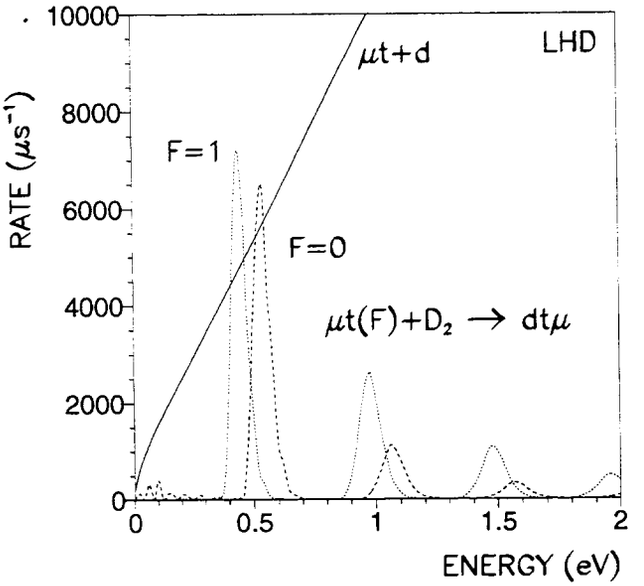

Figure 4: Rates of the $\mu t + d$ collisions and $dt\mu$ resonant formation in the reaction $\mu t(F) + D_2$ *vs.* laboratory energy of the μt atom (LHD).

[30, 31], and the transfer rate $\mu p \rightarrow \mu t$ $\lambda_{pt} = 5.5 \cdot 10^3 \mu s^{-1}$ [21]. The $dt\mu$ fusion rate $\lambda_f = 10^6 \mu s^{-1}$ is much larger than the other rates due to a resonance mechanism of the dt fusion [32].

3 Results of Monte Carlo Calculations

3.1 Kinetics Calculations

The kinetics equations were solved by the Monte Carlo method using the universal kinetics code developed recently at Kurchatov Institute [26, 33]. For the present calculations a new version of the code was used which allows one to solve kinetics problems in inhomogeneous systems. For a given setup, from 10^6 to $4 \cdot 10^6$ chains of the events were usually generated, the accuracy of the results being sufficient for comparison with the expected experimental data.

3.2 Emission of Muonic Tritium

In this section we consider how the yield and the energy spectrum of the muonic tritium emission depend on the thickness of the H-T layer, the tritium fraction, and the thickness of the covering deuterium layer. Two issues determine the optimum parameters of the H-T layer. First, the thickness of the hydrogen layer must be comparable with the mean

range of muonic tritium in hydrogen in the energy range of the Ramsauer-Townsend effect, as it was already shown in Sec. 2.1. Second, since the muon transfer from hydrogen to tritium competes with the $pp\mu$ molecule formation, in order to prevent the muons from being trapped in $pp\mu$ states the tritium fraction must be chosen according to the following estimation

$$C_t \geq C_p \frac{\lambda_{pp\mu}}{\lambda_{pt}} \approx 0.4 \cdot 10^{-3} \tag{3}$$

The calculated dependence of the $t\mu$ emission into vacuum and the yields of the $pp\mu$, $pt\mu$, and $dt\mu$ formation on the tritium fraction in the production target are shown in Figures 5 and 6.

The μt yield per muon stop is a monotonically decreasing function of the layer thickness due to the muon loss in the $pt\mu$ formation, with the upper limit being determined by the probability of the muon transfer from hydrogen to tritium. In practice, due to a momentum spread of the muon beam, the muon stop rate increases with increasing thickness of the production target, and the *absolute* yield of the emitted μt atoms reaches its maximum at some finite thickness.

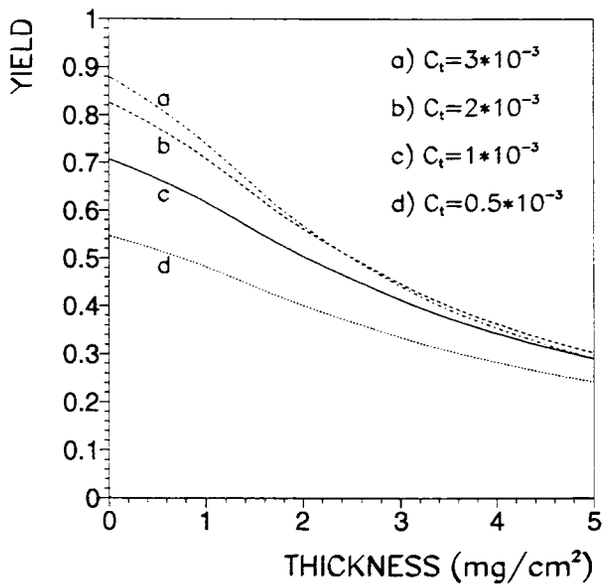

Figure 5: The yields of μt emission into vacuum per muon stop *vs.* the thickness of the production target at various tritium fractions: $C_t = 3 \cdot 10^{-3}$ (a), $2 \cdot 10^{-3}$ (b), 10^{-3} (c), $0.5 \cdot 10^{-3}$ (d) (without the US deuterium overlayer).

With increasing tritium fraction, the yield of the μt emission goes to saturation at $C_t \sim 10^{-3}$, when muon transfer to tritium starts to dominate the μp disappearance rate, and the side process of $pp\mu$ formation gets suppressed.

As already mentioned in Sec. 1, the energy spectrum of the emitted μt must have an enhancement in the region of the Ramsauer-Townsend effect in $\mu t + p$ scattering. The calculations confirm this expectation as shown in Fig. 7(a): the main part of the energy

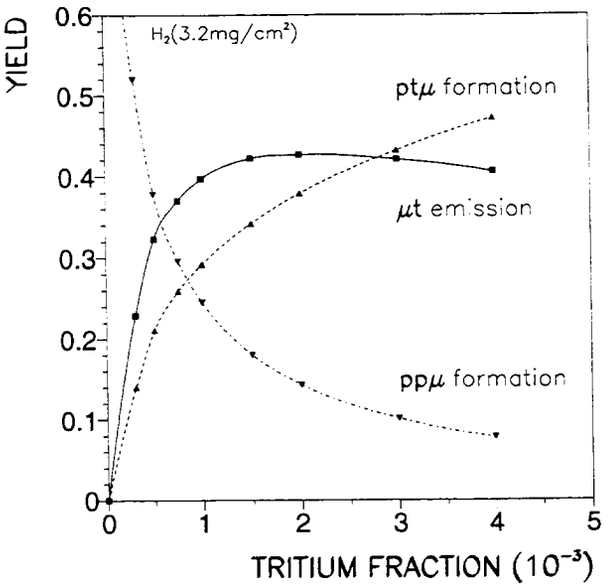

Figure 6: The yields of μt emission into vacuum and the formation of $pp\mu$ and $pt\mu$ molecules per muon stop *vs.* the tritium fraction in the production target of 3.2 mg/cm^2 thickness (without the US deuterium overlayer).

distribution is localized around the minimum in the $\mu t + p$ cross section (see Fig. 3). Other features of the energy distribution in Fig. 7(a) are: a small peak at $E \approx 45$ eV due to muon transfer from hydrogen to tritium and a low energy component representing partial thermalization.

The energy distribution of the emitted μt atoms can be experimentally investigated by measuring the time distributions for the reactions induced by μt travelling through the vacuum gap to the secondary target (DS), such as $dt\mu$ formation[3]. In the case of resonant $dt\mu$ formation the reaction rate is very high, and the measured time distribution is mainly determined by the time of flight.

The muon decay during the time of flight between the production target (US) and the main fusion target (DS) depletes the low-energy part of the energy distribution (Fig. 7(a)). However, for a gap of a few cm the energy distribution of the projectiles preserves the structure determined by the Ramsauer-Townsend effect, and it is clearly visible in the dt fusion time distribution shown in Fig. 7(b). Due to angular divergence of the emitted beam (see below) there is no unique correspondence between the time of flight and the kinetic energy, but the angular distribution can be well defined, if necessary, by placing a collimator between the production and secondary targets. For given kinetic energy E and diffusion-like angular distribution $dw/d\cos\theta \sim \cos\theta$ the mean time of flight through

[3]It is worthwhile to note that for this kind of measurement the reactions of the muon transfer to elements $Z > 1$ can be used as well.

the gap of width l is given by the formula

$$t = \frac{2l}{(2E/M_{\mu t})^{1/2}} = 2.8\, l \cdot E^{-1/2} \ \ \mathrm{cm}^{-1}\mathrm{eV}^{1/2}\,\mu\mathrm{s} \tag{4}$$

where $M_{\mu t}$ is the μt atom mass. With this estimation one can easily verify that the mean time $\bar{t} = 1.3\,\mu$s in the time distribution in Fig. 7(b) corresponds to energy $E = 14\,$eV, which is close to the mean energy $\bar{E} = 13.7\,$eV for the energy distribution plotted in Fig. 7(a).

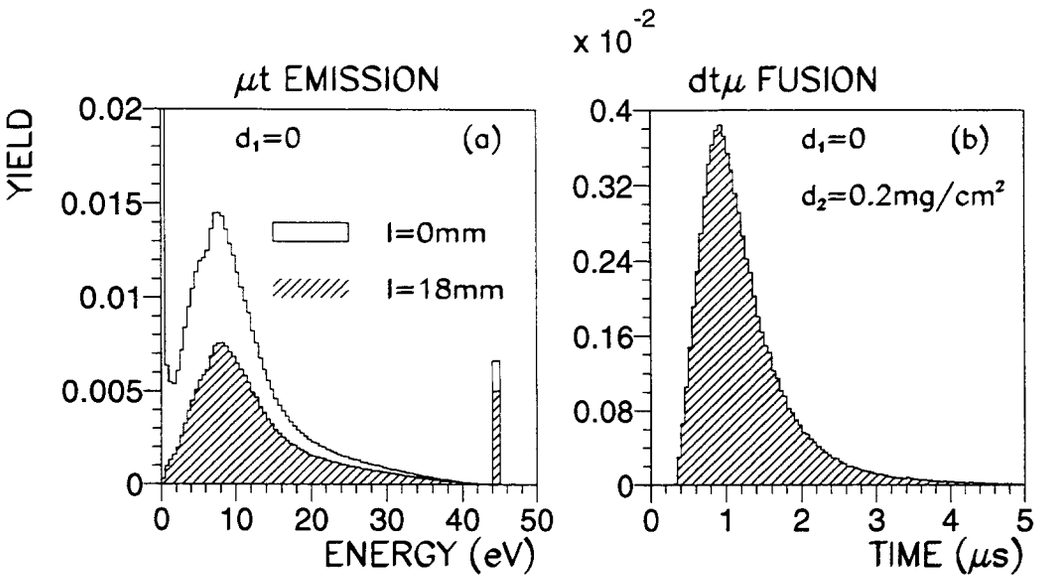

Figure 7: (a) The energy distribution of the μt emitted from an H-T layer of 3.2 mg/cm^2 ($C_t = 10^{-3}$) at the layer surface (light) and at the distance $l = 18\,$mm (shaded). (b) The dt fusion time distribution for the fusion target (DS) of 0.2 mg/cm^2 at $l = 18\,$mm.

For measuring the energy dependence of the $dt\mu$ formation rates one needs an atomic beam of much smaller energy than is provided by the Ramsauer-Townsend effect. A deuterium overlayer (US) of thickness of a few interaction lengths can be used for degrading the emitted muonic atoms, as is demonstrated in Figures 8 and 9.

With increasing thickness of the deuterium layer, some depletion of the energy distribution in the region of a strong resonance formation ($E_{lab} \sim 0.5$eV) becomes noticeable (see Fig. 9), however a fast feeding due to elastic collisions $\mu t + d$ prevents a complete depletion of the resonance region of the energy distribution.

The muon decay during the time of flight between the production and fusion target significantly reduces the low-energy part of the kinetic energy distribution for μt atoms arriving at the fusion target. The mean kinetic energy of the μt atoms arriving at the DS deuterium layer ($l = 18mm$) changes with the thickness of the US layer as follows: $\bar{E}(0\,\mu\mathrm{g/cm}^2) = 14$eV, $\bar{E}(19\,\mu\mathrm{g/cm}^2) = 6.2$eV, $\bar{E}(58\,\mu\mathrm{g/cm}^2) = 2.2$eV, $\bar{E}(94\,\mu\mathrm{g/cm}^2) = 1.3$eV.

The uniformity of the covering layer is important for precision measurements; a 10% variation of the thickness of the US layer of $58\,\mu g/cm^2$ results in about 20% variation of the yield of the μt atoms and in about 0.3 eV variation of the mean kinetic energy at the DS layer.

The deuterium overlayer reduces the μt emission due to the absorption via $dt\mu$ formation and the reflection of the μt atoms back into the H-T layer, the dependence of the yields of the emission and the $dt\mu$ and $pt\mu$ formation on the thickness being demonstrated in Fig. 10.

The dependence of μt emission into vacuum and the yields of the $pp\mu$, $pt\mu$, and $dt\mu$ formation on the tritium fraction in the production target for the covering deuterium layer of $58\,\mu g/cm^2$ are shown in Fig. 11.

The dependence of the angular distribution of the emitted μt atoms on the distance from the production target and the thickness of the US deuterium layer is shown in Fig. 12. When the time of flight becomes large in comparison with the muon lifetime, the angular distribution is more localized near the z-axis with increasing the distance from the production target, because the shortest trajectories are less likely to be lost due to the decay.

The summary of the calculated fusion yields for various thicknesses of the deuterium layers and the tritium fraction is given in Table 1 (the statistical errors are not shown, but in all cases they do not exceed a unit in the last digit).

3.3 $dt\mu$ Formation in the Upstream Deuterium Layer

The $dt\mu$ molecule formation in the deuterium overlayer can be used for investigation of transfer from hydrogen to tritium. Figure 13 shows the calculated time dependence of dt fusion in the relatively thick (0.2 mg/cm^2) US layer at various tritium fractions $C_t = 0.5 \cdot 10^{-3}$, $10^{-3}, 2 \cdot 10^{-3}$. At large time ($t > 0.1\,\mu s$) the spectrum is determined by the disappearance rate of muonic hydrogen:

$$\Lambda_{\mu p} = \phi(C_t \lambda_{pt} + C_p \lambda_{pp\mu}) + \lambda_0 \tag{5}$$

Both the $\mu p \rightarrow \mu t$ transfer rate λ_{pt} and the $pp\mu$ formation rate $\lambda_{pp\mu}$ can be determined from the set of measurements at different tritium fractions C_t.

The build-up structure is mainly determined by μt diffusion in the H-T layer since the slowing down of the 'hot' μt into the resonance $dt\mu$ formation region in deuterium is fast (compare Figures 3 and 4).

3.4 $dt\mu$ Formation in the Downstream Deuterium Layer

Measuring the energy dependence of the $dt\mu$ formation rate by the ToF method is a difficult task, because this kind of inverse problem is known to be ill-defined. In this situation, the data analysis essentially relies on a theoretical input that makes the problem well-defined. From the physical viewpoint, there are two obstacles to be overcome in obtaining a clear signal from resonant formation, as it is predicted by the current theory, in

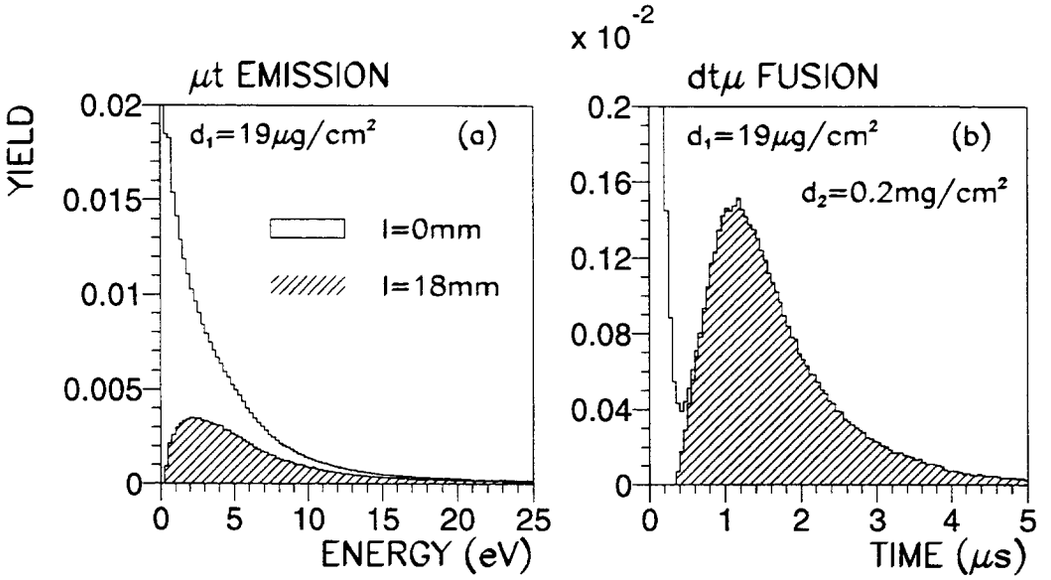

Figure 8: (a) The energy distribution of the μt, emitted from an H-T layer of 3.2 mg/cm^2 ($C_t = 10^{-3}$) covered with a deuterium layer (US) of 19.4 μg/cm^2, at the layer surface (light) and at the distance $l = 18$ mm (shaded). (b) The dt fusion time distribution. The shaded area shows the contribution of the main fusion target (DS) ($d_2 = 0.2$ mg/cm^2, $l = 18$ mm).

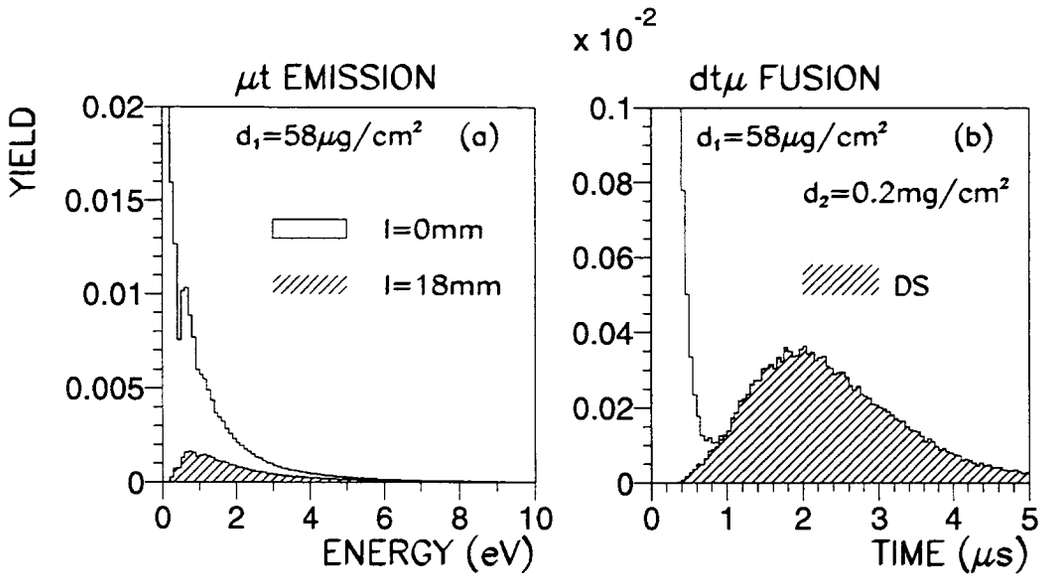

Figure 9: (a) The energy distribution of the μt, emitted from an H-T layer of 3.2 mg/cm^2 ($C_t = 10^{-3}$) covered with a deuterium layer (US) of 58 μg/cm^2, at the layer surface (light) and at the distance $l = 18$ mm (shaded). (b) The dt fusion time distribution. The shaded area shows the contribution of the main fusion target (DS) ($d_2 = 0.2$ mg/cm^2, $l = 18$ mm).

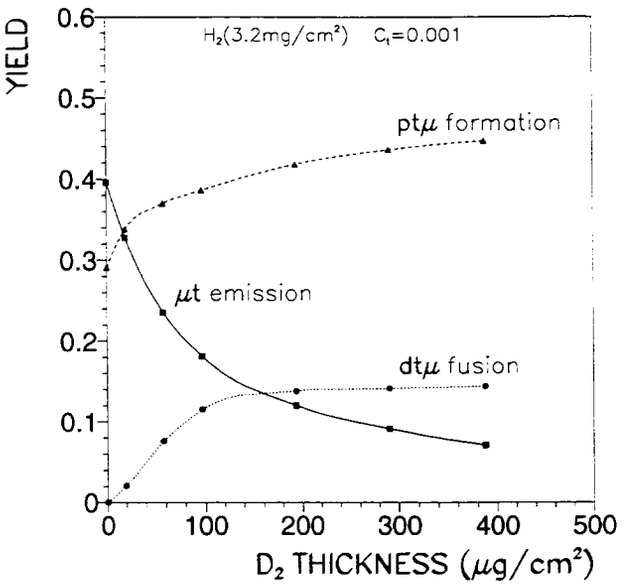

Figure 10: The yields of μt emission into vacuum and the $pt\mu$ and $dt\mu$ molecular formation *vs.* the thickness of the US deuterium layer ($C_t = 10^{-3}$).

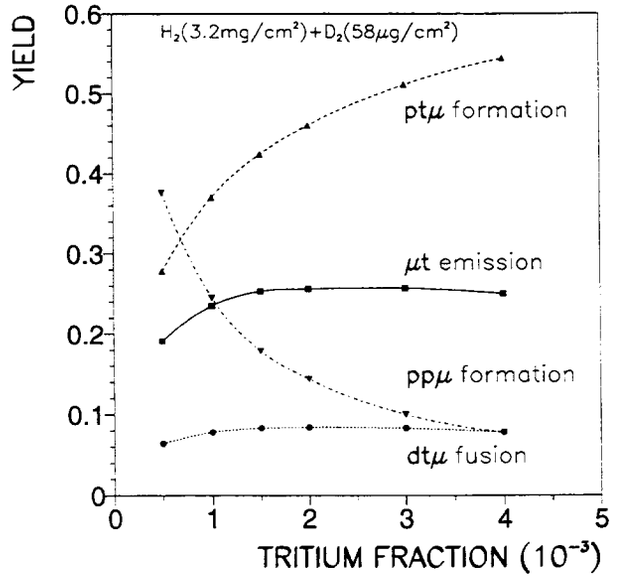

Figure 11: The yields of μt emission into vacuum and the formation of $pp\mu$, $pt\mu$, and $dt\mu$ molecules per muon stop *vs.* the tritium fraction in the production target (the thickness of the US deuterium layer $l_1 = 58\,\mu\mathrm{g/cm^2}$).

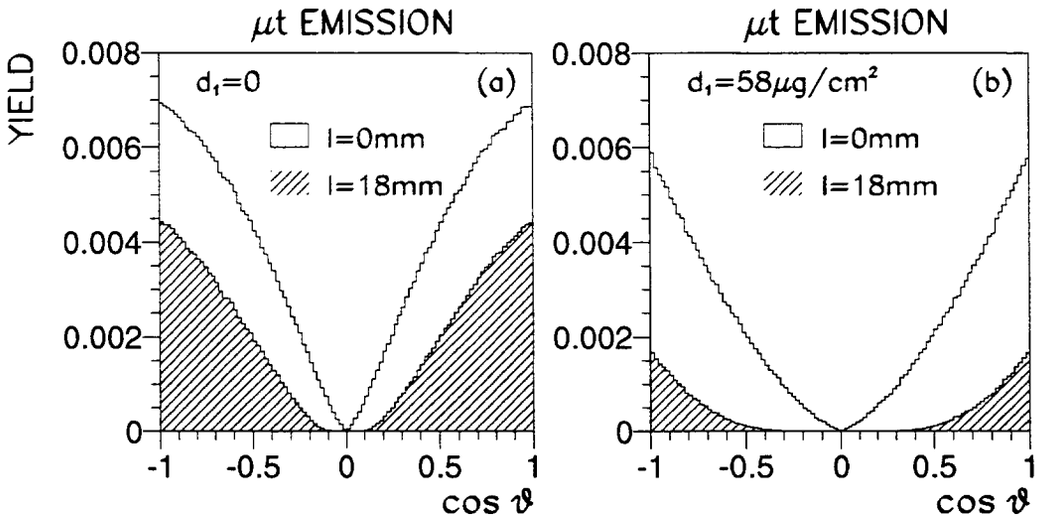

Figure 12: The angular distribution of the emitted μt atoms at $l = 0\,\mathrm{mm}$ (light) and $l = 18\,\mathrm{mm}$ (shaded): (a) – without the US deuterium layer, (b) – for the US deuterium layer of 58 $\mu\mathrm{g/cm^2}$.

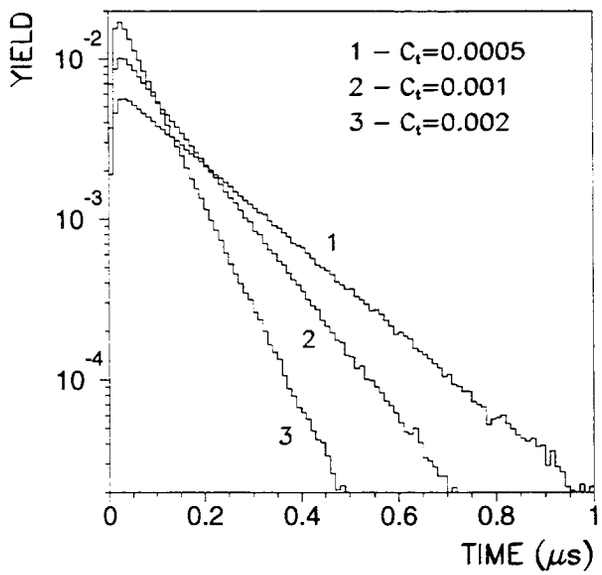

Figure 13: The time distributions of $dt\mu$ fusion in a thick US deuterium layer of 0.2 $\mathrm{mg/cm^2}$ for various tritium fractions ($C_t = 0.5 \cdot 10^{-3}$, 10^{-3}, $2 \cdot 10^{-3}$).

Table 1: The yields of μt emission and $dt\mu$ fusion *vs.* the thicknesses of the deuterium layers d_1 (US) and d_2 (DS) and tritium fraction C_t: $Y_1(\mu t)$ – the total μt emission from the production target, $Y_2(\mu t)$ – the μt arriving at the main fusion target, $Y(dt\mu)$ – the total fusion in $dt\mu$, $Y_1(dt\mu)$ – the $dt\mu$ fusion in the D_2 layer on the production target, $Y_2(dt\mu)$ – the $dt\mu$ fusion in the main fusion target. The thickness of the H-T layer is 3.2 mg/cm^2. The yields are normalized per muon stop in the H-T layer, but include emission from two sides of the layer, rather than one as is typical in an experiment.

d_1 μg/cm^2	d_2 μg/cm^2	C_t	Y_1	Y_2	$Y(dt\mu)$	$Y_1(dt\mu)$	$Y_2(dt\mu)$
0.	0.	0.001	0.397	0.202	0.	0.	0.
19.	0.	0.001	0.327	0.113	0.021	0.021	0.
58.	0.	0.001	0.235	0.037	0.079	0.079	0.
97.	0.	0.001	0.181	0.011	0.115	0.115	0.
58.	0.	0.0005	0.190	0.030	0.064	0.064	0.
58.	0.	0.002	0.256	0.040	0.084	0.084	0.
58.	0.	0.003	0.255	0.039	0.082	0.082	0.
58.	0.	0.004	0.248	0.038	0.079	0.079	0.
19.	19.	0.001	0.327	0.113	0.029	0.021	0.007
19.	58.	0.001	0.327	0.113	0.048	0.021	0.026
19.	97.	0.001	0.327	0.113	0.060	0.021	0.038
19.	194.	0.001	0.327	0.113	0.067	0.021	0.046
58.	19.	0.001	0.235	0.037	0.083	0.079	0.0036
58.	58.	0.001	0.235	0.037	0.089	0.079	0.010
58.	97.	0.001	0.235	0.037	0.093	0.079	0.014
58.	194.	0.001	0.235	0.037	0.095	0.079	0.016

the setup concerned. First, the muonic tritium emission based on the Ramsauer-Townsend effect produces μt with the kinetic energy that is much higher than the resonance one. Second, since the μt deceleration rate increases with energy, $dt\mu$ formation can follow the fast slowing down in elastic collisions, and this 'feeding' effect make it impossible to use a naive interpretation of the ToF spectra.

Figure 14 demonstrates these features of $dt\mu$ formation in the US deuterium layer of 19 mg/cm^2 (the energy distribution of the μt atoms at the instant of reaching the DS target is shown in Fig. 8).

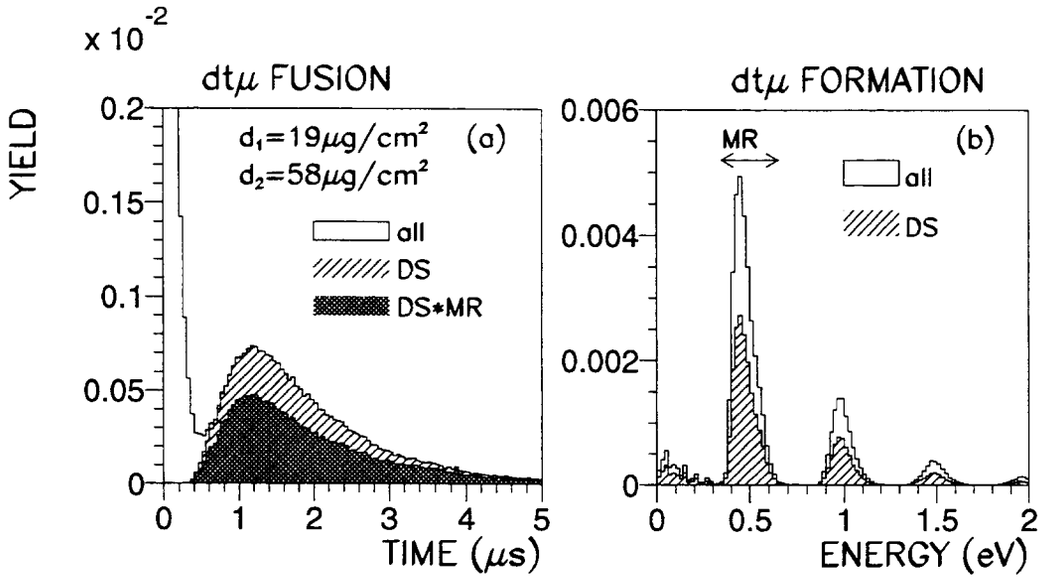

Figure 14: The time distributions of the $dt\mu$ fusion (a) and the energy distribution of the μt atoms at the instant of the $dt\mu$ formation (b) for the US layer of 19 μg/cm^2 and the DS layer of 58 μg/cm^2. The contribution of the DS layer is shaded, with the dark shade showing the contribution of the main resonances ($0.35\,\mathrm{eV} < E < 0.65\,\mathrm{eV}$).

The feeding can be reduced by decreasing the thickness of the DS layer to 1–2 interaction lengths in the resonance formation region and by increasing the thickness of the US layer to degrade most of the μt atoms to the energy range of the resonance formation, as is demonstrated in Figures 15 and 16. As soon as sufficient statistics can be accumulated, a clear signal from the main resonances ($E \sim 0.5$ eV, see Fig. 4) can be seen in the fusion time distributions at large time $t > 3.5\,\mu$s. The higher resonances ($E \approx 1$eV) produce a significant contribution to the fusion time distribution at $t = 2 - 3\,\mu$s because of the enhancement of the initial energy distribution of the μt atoms in this region (see Fig. 9(a)).

The accuracy of the present calculations of the fusion time spectra is limited by current uncertainties in the $dt\mu$ formation rates. Our results have been obtained with the rates calculated in the dipole approximation [10], which appears to overestimate the rates by factor of about 2, according to recent studies of the kinetics of $dt\mu$ fusion cycle [27, 28]

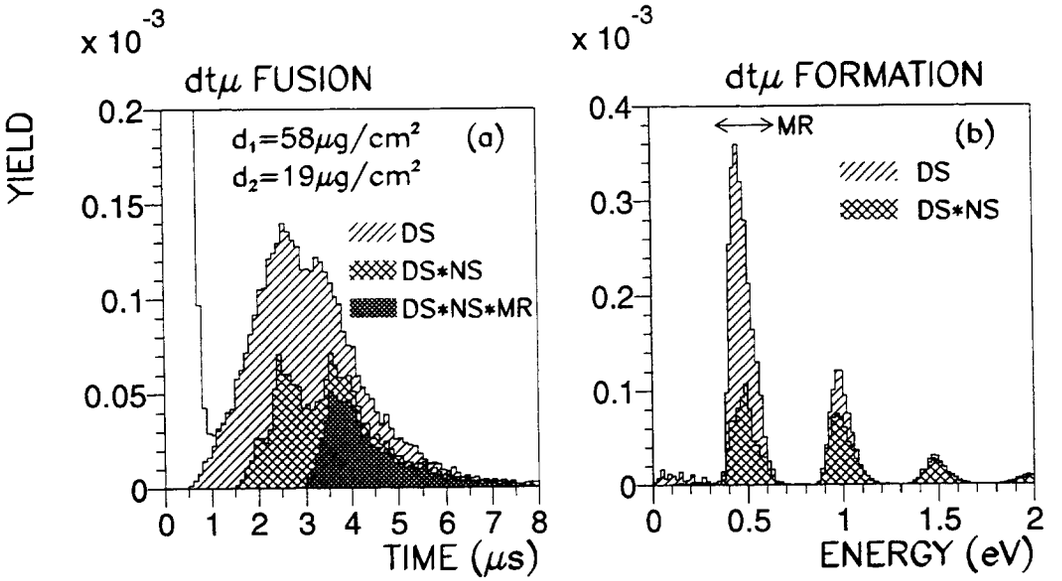

Figure 15: The time distributions of $dt\mu$ fusion (a) and the energy distribution of the μt atoms at the instant of the $dt\mu$ formation (b) for the US layer of 58 μg/cm^2 and the DS layer of 19 μg/cm^2. The contribution of the DS layer is light shaded. The direct $dt\mu$ formation in the DS layer is medium shaded, with the dark shade showing the contribution of the main resonances ($0.35\,\mathrm{eV} < E < 0.65\,\mathrm{eV}$).

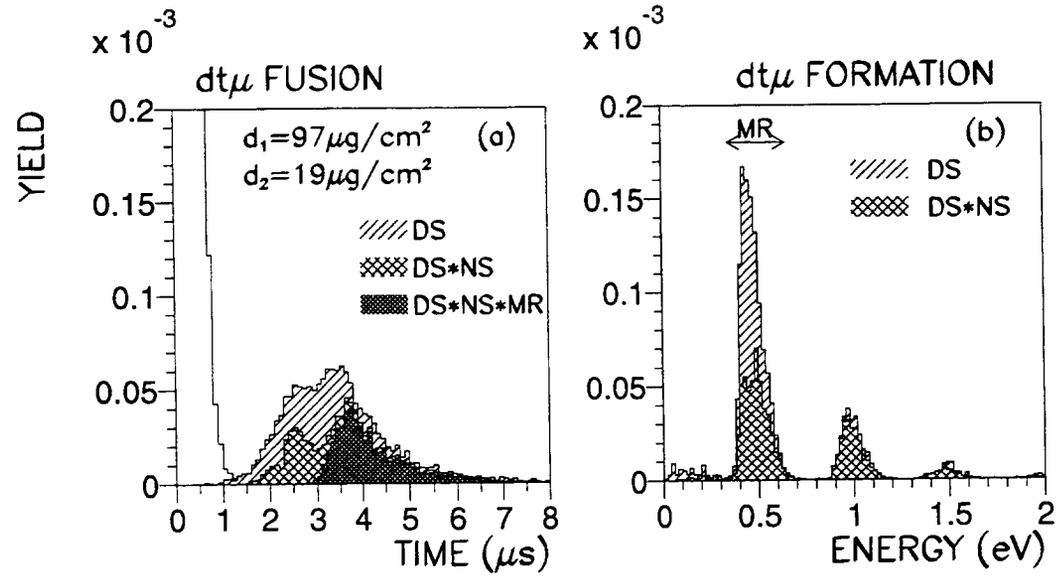

Figure 16: The time distributions of the $dt\mu$ fusion (a) and the energy distribution of the μt atoms at the instant of the $dt\mu$ formation (b) for the US layer of 97 μg/cm^2 and the DS layer of 19 μg/cm^2. The contribution of the DS layer is light shaded. The direct $dt\mu$ formation in the DS layer is medium shaded, with the dark shade showing the contribution of the main resonances ($0.35\,\mathrm{eV} < E < 0.65\,\mathrm{eV}$).

and more refined calculations at $T = 30 - 300\,\mathrm{K}$ [11]. In order to account for these uncertainties, one can use a factor k_{form} multiplying all $dt\mu$ formation rates. The calculations for a very thin reaction (DS) layer, which is of main interest for measuring the formation rates, show that for $k_{form} = 0.5 - 1$ the main features of the kinetics, including the shape of fusion time distribution, are preserved, while the probability of $dt\mu$ formation decreases from $Y_2 = 1.45 \cdot 10^{-3}$ at $k_{form} = 1$ to $Y_2 = 0.81 \cdot 10^{-3}$ at $k_{form} = 0.5$ for the setup parameters corresponding to Fig. 16.

4 Conclusion

In conclusion, the results of the kinetics calculations can be summarized as follows.

1. A protium layer of a few mg/cm^2 thickness with a small admixture of tritium ($C_t \sim 10^{-3}$) can efficiently convert the stopped muons into a beam of μt atoms emitted from its surface into vacuum.

2. The energy distribution of the emitted μt features the characteristic peak at the laboratory energy $E \sim 10\,\mathrm{eV}$ with width of a few eV, which corresponds to the minimum in the elastic cross section for the $\mu t + p$ scattering due to the Ramsauer-Townsend effect.

3. The time-of-flight method can be applied for determining the energy distribution of the emitted atoms, allowing one to check the current theoretical calculations of the cross sections.

4. A covering deuterium layer of a few interaction lengths can be used to degrade the emitted atoms. The overlayer of about 0.1 mg/cm^2 provides a rather slow atomic beam with a mean kinetic energy of about 1 eV which is optimal for measuring the energy dependence of the $dt\mu$ molecule formation rates with the time of flight method.

5. The efficiency of the muonic tritium emission into vacuum is already close to saturation at a tritium concentration $C_t = 10^{-3}$, and the further increase of C_t is useful only for the improvement of the time resolution due to shortening of the time of the muon transfer from a proton to a triton.

6. With the setup consisting of a main production layer and a thick deuterium overlayer one can measure the $pp\mu$ molecular formation rate and the rate of the transfer $\mu p \to \mu t$ by measuring the time distribution of dt fusion for the set of measurements at various tritium concentration in the main production target $C_t = 0.5 \cdot 10^{-3} - 2 \cdot 10^{-3}$.

7. In measuring the energy dependence of the muonic molecule formation rates by the ToF method, the thickness of the downstream fusion target must be small enough (about one interaction length for the resonant formation cross section) to reduce the contribution from slowing down before the muonic molecule formation.

8. The muon decay in the vacuum gap of a few cm rejects the longer trajectories and thus makes the angular distribution of the low energetic muons arriving at the downstream target concentrated near the perpendicular to the surface.

9. The comparison of the kinetics calculations with the experimental data from the current TRIUMF experiment [17] and future ones based on the setup considered provides a new way for a comprehensive test of the theoretical results concerning the energy dependence of various reactions with muonic atoms and molecules, yet to be exploited.

5 Acknowledgments

The author wishes to thank Dr. G.M. Marshall for kind hospitality at TRIUMF where part of this work was done, the members of Muonic Hydrogen Collaboration for numerous fruitful discussions, and Prof. L.I. Ponomarev and Dr. M.P. Faifman for providing the tables of the $dt\mu$ formation rates. This work was supported in part by the NATO Linkage Grant LG 930162. The software used for the kinetics calculations was developed with partial support by the U.S. National Science Foundation Grant No. NSF PHY-9115407.

References

[1] Int. Conf. on Muon Catalyzed Fusion μCF-90, (Vienna, 1990), Muon Catalyzed Fusion, **6/7**, (1990/91); Int. Workshop. on Muon Catalyzed Fusion μCF-92, (Uppsala, 1992), Hyperfine Interactions **92** (1993).

[2] S.S. Gerstein, Yu.V. Petrov, L.I. Ponomarev, Usp. Fiz. Nauk **160** (1990) 3 [Sov. Phys. Usp. **33** (1990) 591].

[3] L.I. Ponomarev and C. Petitjean, Fusion Technology **20** (1991) 1022.

[4] J.S. Cohen, Atomic and Molecular Processes in Muon Catalyzed Fusion, in *Review of Fundamental Processes and Applications of Atoms and Ions, Ch.2*, Ed. C.D. Lin, World Scientific, Singapore, 1993.

[5] S.E. Jones, A.N. Anderson, A.J. Caffrey, C. DeW. Van Siclen, K.D. Watt, J.N. Bradbury, J.S. Cohen, P.A.M. Gram, M. Leon, H.R. Maltrud, and M.A. Paciotti, Phys. Rev. Lett. **51** (1983) 1757.

[6] C. Petitjean, Nucl. Phys. **A543** (1992) 79c.

[7] E.A. Vesman, Pisma ZhETF **5** (1967) 113 [JETP Lett. **5** (1967) 91].

[8] S.S. Gerstein and L.I. Ponomarev, Phys. Lett. **72B** (1977) 80.

[9] M.P. Faifman, L.I. Menshikov, and T.A. Strizh, Muon Catalyzed Fusion **4** (1989) 1.

[10] M.P. Faifman and L.I. Ponomarev, Phys. Lett. **B265** (1991) 201.

[11] Yu.V. Petrov, V.Yu. Petrov, H.H. Schmidt, Phys. Lett. **B331** (1994) 266.

[12] V.M. Bystritskii, V.P. Dzhelepov, Z.V. Ershova, V.G. Zinov, V.K. Kapyshev, S.Sh. Mukhamet-Galeeva, V.S. Nadezhdin, L.A. Rivkis, A.I. Rudenko, V.I. Satarov, N.V. Sergeeva, L.N. Somov, V.A. Stolupin, and V.V. Filchenkov, ZhETF **80** (1982) 1700 [Sov. Phys. JETP **53** (1982) 877].

[13] S.E. Jones, A.N. Anderson, A.J. Caffrey, C. DeW. Van Siclen, K.D. Watt, J.N. Bradbury, J.S. Cohen, P.A.M. Gram, M. Leon, H.R. Maltrud, and M.A. Paciotti, Phys. Rev. Lett. **56** (1986) 588.

[14] W.H. Breunlich, M. Cargnelli, P. Kammel, J. Marton, N. Nägele, A. Scrinzi, J. Werner, J. Zmeskal, J. Bistirlich, K.M. Crowe, M. Justice, J. Kurck, C. Petitjean, R.H. Sherman, H. Bossy, H. Daniel, F.J. Hartmann, W. Neumann, G. Schmidt, and T. von Egidy, Muon Catalyzed Fusion **1** (1987) 67.

[15] P. Kammel, P. Ackerbauer, W.H. Breunlich, M. Cargnelli, M. Jeitler, J. Marton, N. Nägele, A. Scrinzi, J. Werner, J. Zmeskal, C. Petitjean, J. Bistirlich, K.M. Crowe, M. Justice, R.H. Sherman, H. Bossy, H. Daniel, F.J. Hartmann, H. Plendl, W. Schott, and W. Neumann, Muon Catalyzed Fusion **3** (1988) 483.

[16] B.M. Forster, J.M. Bailey, G.A. Beer, J.L. Beveridge, J.H. Brewer, W.N. Hardy, T.M. Huber, K.R. Kendall, A.R. Kunselman, J.A. Macdonald, G.M. Marshall, G.R. Mason, A. Olin, M. Senba, and J.B. Warren, Hyperfine Interactions **65** (1990) 1007.

[17] G.M. Marshall, J.L. Beveridge, J.M. Bailey, G.A. Beer, P.E. Knowles, G.R. Mason, A. Olin, J.H. Brewer, B.M. Forster, T.M. Huber, B. Pippitt, R. Jacot-Guillarmod, L. Schellenberg, P. Kammel, J. Zmeskal, A.R. Kunselman, C.J. Martoff, and C. Petitjean, Hyperfine Interactions **82** (1993) 529.

[18] L.W. Alvarez, H. Bradner, F.S. Crawford, J.A. Crawford, P. Falk-Variant, M.L. Good, J.D. Gow, A.H. Rosenfeld, F. Solmitz, M.L. Stevenson, H.K. Ticho, and R.D. Tripp, Phys. Rev. **105** (1957) 1127.

[19] M. Bubak and M.P. Faifman, Preprint JINR E4-87-464 (1987).

[20] C. Chiccoli, V.I. Korobov, V.S. Melezhik, P. Pasini, L.I. Ponomarev, and J. Wozniak, Muon Catalyzed Fusion **7** (1992) 87.

[21] J.S. Cohen and M.C. Struensee, Phys. Rev. **A43** (1991) 3460.

[22] J.S. Cohen and M. Leon, Phys. Rev. Lett. **55** (1985) 52.

[23] P. Kammel, Nuovo Cim. Lett. **43** (1985) 349.

[24] W.H. Breunlich, P. Kammel, J.S. Cohen and M. Leon, Ann. Rev. Nucl. and Part. Sci. **39** (1989) 311.

[25] M. Jeitler, W.H. Breunlich, M. Cargnelli, P. Kammel, J. Marton, N. Nägele, P. Pawlek, A. Scrinzi, J. Werner, J. Zmeskal, H. Daniel, F.J. Hartmann, G. Schmidt, T. von Egidy, C. Petitjean, J. Bistirlich, H. Bossy, K.M. Crowe, M. Justice, J. Kurck, R.H. Sherman, and W. Neumann, Muon Catalyzed Fusion **5/6** (1990/91) 217.

[26] V.E. Markushin, E.I. Afanasieva, and C. Petitjean, Muon Catalyzed Fusion **7** (1992) 155.

[27] V.E. Markushin, E.I. Afanasieva, T. Case, K. Lou, and C. Petitjean, Hyperfine Interactions **82** (1993) 373.

[28] M. Jeitler, W.H. Breunlich, M. Cargnelli, P. Kammel, J. Marton, N. Nägele, P. Pawlek, A. Scrinzi, J. Werner, J. Zmeskal, H. Bossy, H. Daniel, F.J. Hartmann, G. Schmidt, T. von Egidy, C. Petitjean, J. Bistirlich, K.M. Crowe, M. Justice, J. Kurck, R.H. Sherman, and W. Neumann, Hyperfine Interactions **82** (1993) 391.

[29] E.J. Bleser, E.W. Anderson, L.M. Lederman, S.L. Meyer, J.L. Rosen, J.E. Rothberg, I-T. Wang, Phys. Rev. **132** (1963) 2679.

[30] L.I. Ponomarev and M.P. Faifman, ZhETF **71** (1976) 1689 [Sov. Phys. JETP **44** (1976) 886].

[31] M.P. Faifman, Muon Catalyzed Fusion **4** (1989) 341.

[32] L.N. Bogdanova, V.E. Markushin, and V.S. Melezhik, ZhETF **81** (1981) 829 [Sov. JETP **54** (1981) 442].

[33] V.E. Markushin (unpublished).